

Noninvasive Sensor for Continuous Intraocular Pressure Monitoring

Shujing Su,^{1,2#} Lei Zhang,^{1,2#} Gao Fei,³ Lei Fan,^{1,2}
Helei Dong,^{1,2} Qiulin Tan,^{1,2*} Jijun Xiong,^{1,2} and Sanmin Shen^{1,2}

¹Key Laboratory of Instrumentation Science & Dynamic Measurement,
North University of China, Ministry of Education, Tai Yuan 030051, China

²Science and Technology on Electronic Test and Measurement Laboratory,
North University of China, Tai Yuan 030051, China

³Xianyang Office, Xi'an Military Representative Bureau, PLAGF

(Received June 21, 2018; accepted October 22, 2018)

Keywords: IOP, LC resonant, inductor coils, PDMS, MEMS

Pathological elevated intraocular pressure (IOP) is a primary index for glaucoma. In this paper, we present a biocompatible IOP sensor that operates based on the principle of inductor-capacitor (LC) resonance. The IOP sensor is composed solely of a spiral inductor that can sense deformations of corneal curvature. The inductor is fabricated by embedding gold coils into polydimethylsiloxane (PDMS), a soft, biologically compatible material, via MEMS technology. The resonant frequency of the sensor is designed to vary when the IOP is changed in experiments. The frequency response of the sensor is tested using a model eye, a tube, and a network analyzer. The results show that there is approximately linearity between the frequency response of the sensor and the IOP. The sensitivity of the sensor is 417.29 kHz/mmHg, when the pressure ranges from 7.5 to 36.88 mmHg. Consequently, an unstable IOP could be accurately tracked, using the calibrated relationship between frequency response and the IOP.

1. Introduction

Glaucoma is the second major cause of blindness globally, with excessive intraocular pressure (IOP) being a key risk factor of this condition.⁽¹⁾ The IOP is usually in the 10–21 mmHg range (1.33–2.80 kPa), which is sufficient for maintaining the wall tension of the eyeball and a constant corneal surface curvature.^(2–3) When the IOP increases beyond this range, the optic nerve will be oppressed and gradually atrophy. This atrophy can eventually lead to glaucoma, which can cause blindness.⁽⁴⁾ By 1957, the applanation tonometer designed by Goldmann, had become an important IOP assessment tool because of its ability to perform accurate and reliable measurements.⁽⁴⁾ The use of the Goldmann tonometer is thus considered the standard measurement technique for glaucoma. However, this device is not suitable for the real-time measurement of the IOP, as it is not portable or wearable.⁽⁵⁾

In recent years, many institutions around the world have studied IOP detection. The IOP can be measured by implanting telemetric pressure sensors into the eye. In 2012, Chitnis'

*Corresponding author: e-mail: tanqiulin@nuc.edu.cn

#These authors contributed equally to this work.

<https://doi.org/10.18494/SAM.2018.1991>

group from Purdue University inserted a microneedle into the sclera of an eye and connected this to a capacitive sensor. The aqueous humor squeezes capacitor plates via the microneedle, causing changes to the resonant frequency of the sensor, when the internal pressure of the sclera is high;⁽⁶⁾ however, in Chitnis' design, a pressure sensor had to be implanted into the eye through minimally invasive surgery, which is unacceptable to most healthy people as it can cause eye inflammation. The Guozhen Chen group from The Hong Kong University of Science and Technology reported a contact lens IOP sensor, with inductor coils connected to capacitor plates, placed on the surface of an eye. The variation in inductance, caused by the changes in corneal curvature, leads to changes in resonant frequency.⁽⁷⁾ However, the sensitivity of the device is 8 kHz/mmHg and can be easily influenced by noise and error caused by eye movements and blinking. The Chiou's group from National Chiao Tung University proposed a capacitor-based sensor for IOP monitoring. The sensitivity of this device is 1.2239 pF/mmHg for pressures between 18 and 30 mmHg.⁽⁴⁾ Because of its complex structure, it is difficult to achieve mass production and its practical application is limited. Ghaed *et al.* developed a cubic-millimeter energy-autonomous wireless IOP monitor. Their design achieves zero-net-energy operation with 1.5 h of sunlight or 10 h of bright indoor lighting daily. However, being powered by a solar cell limits its use in 24 h IOP monitoring.⁽⁸⁾ SENSIMED developed a noninvasive IOP measurement system called Triggerfish. The outstanding advantages of this system are that patient intervention is not required for measurements and the noninvasive nature of the device. However, the Triggerfish contact lens is a single-use device and can only be used for a maximum of 24 h, making it unsuitable for the long-term monitoring of the IOP.⁽⁹⁾ Recently, many new IOP sensors have appeared, utilizing emerging materials such as graphene and improved sensor transparency.⁽¹⁰⁾ However, there are still major challenges in terms of long-term biological compatibility.⁽¹¹⁾

We present an IOP sensor with simplified structure and fabrication process compared with the above technologies, as it is composed solely of a spiral inductor coil. Adjacent wires of the coil can be treated as parallel plate capacitors. Thus, a resonant circuit composed of an inductor and a capacitor is formed. The inductor is implanted in biologically compatible and flexible polydimethylsiloxane (PDMS) using MEMS technology. The frequency response of the sensor was tested using a model eye, a tube, and a network analyzer. The resonant frequency was recorded using a network analyzer as the IOP was gradually increased. The results showed that the sensor is approximately linear with respect to frequency response. The sensitivity of the sensor was 417.29 kHz/mmHg when the IOP ranged from 7.5 to 36.88 mmHg. Consequently, the soft contact lens sensor can accurately track an unstable IOP using the calibrated relationship between the frequency response and the IOP.

2. Theory, Design, and Fabrication

2.1 Theory of the IOP sensor

The inductance is noted as L_s . The parasitic capacitance between the coils is C_{par} . The π equivalent model of inductance shows that a resonant frequency, f_0 , appears when the inductance coil and capacitor are connected in series.^(12–14)

$$f_0 = \frac{1}{2\pi\sqrt{L_s C_s}} \quad (1)$$

As reflected in Fig. 1, the inductive antenna emits a frequency sweeping signal, which includes the resonant frequency of the sensor. When the frequency of the signal emitted by the inductive antenna matches the resonant frequency of the sensor, the impedance information (e.g., amplitude and phase) of the antenna is modified. Thus, the resonant frequency can be obtained by extracting the input return loss, S_{11} parameter, which drops to its minimum. The frequency f_m is usually recorded as it is related to the resonant frequency of the sensor through⁽¹³⁾

$$f_m = f_0 \left(1 + \frac{k^2}{4} + \frac{1}{8Q^2} \right), \quad (2)$$

where f_m and Q are the resonant frequency and the quality factor of the sensor, respectively, and k is the inductive coupling coefficient. In the actual test, the mutual inductance between the coils is extremely small and the sensor has a high Q -factor. Thus, the difference between f_m and f_0 is very small, and Eqs. (2) can thus be rewritten as⁽¹⁵⁾

$$f_m \approx f_0. \quad (3)$$

When the IOP changes, the coil bends, modifying the inductance of the sensor, causing changes to the resonant frequency. The inductance of the coil can be obtained using⁽¹⁵⁾

$$L_s = \frac{1}{2} \mu n^2 d_{avg} \left[\ln\left(\frac{2.46}{\rho}\right) + 0.2 \times \rho^2 \right], \quad (4)$$

where μ is the magnetic permeability of vacuum, n is the number of turns in the spiral coil, d_{avg} is the average diameter of the coil, and ρ is the fill ratio of the coil, which is dependent only on

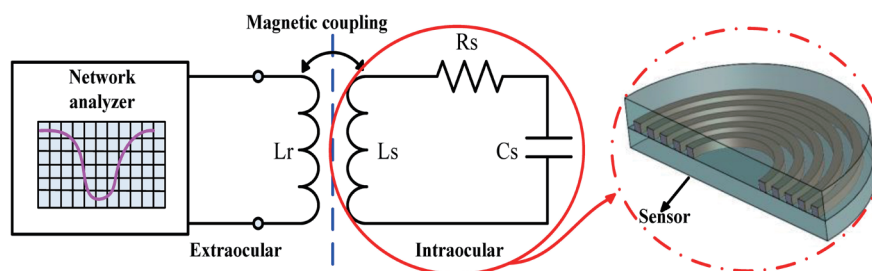


Fig. 1. (Color online) Operational principle of the IOP sensor.

the initial coil width and coil spacing. Thus, ρ can be considered constant, and the average coil diameter changes with the variation of the diameter of each turn when the coil is bent. We can see from the above equation that when the coil is bent, the change in inductance depends only on the change in average diameter.⁽⁶⁾ Equation (4) can thus be simplified to

$$\Delta L_s = m \cdot \Delta d_{avg}, \quad (5)$$

where

$$m = \mu n^2 \frac{[\ln(2.46/\rho) + 0.2 \times \rho^2]}{2}. \quad (6)$$

When the IOP changes, both the average diameter and the radius of curvature of the coil, r , change when the coil is bent. The change in average diameter, Δd_{avg} , and the change in the radius of curvature, Δr , are related as⁽¹⁶⁾

$$\frac{\Delta d_{avg}}{d_{avg}} = a \cdot \Delta r, \quad (7)$$

$$a = \frac{1}{r_0} - \frac{\alpha}{2r_0} \cot\left(\frac{\alpha}{2}\right). \quad (8)$$

Here, r_0 is the initial radius of curvature and α is the initial bending angle. The relationship between the curvature of the eye model and the IOP⁽¹⁷⁾ can be simplified to

$$\Delta r = \Delta p \frac{R_0(1-\nu)}{2Et}, \quad (9)$$

where R_0 is the radius curvature of the model eye, ν is Poisson's ratio of PDMS, and E is the elastic modulus of the PDMS. Thus, when the coil is bent, there is a linear relationship between the change in inductance and the change in the radius of curvature of the coil, in accordance with the above observation.

The parasitic capacitance C_{par} is given by⁽¹⁸⁾

$$C_{par} = \beta \varepsilon_0 \varepsilon_r t_c l_g s, \quad (10)$$

where β is an empirical constant, ε_0 is the vacuum permittivity, and ε_r is the relative permittivity of PDMS. t_c , l_g , and s respectively stand for the wire width, total wire length, and wire thickness, which are invariable, regardless of the deformation of the coil, as shown in Fig. 2. Thus, the capacitance can be regarded as a constant. Coil bending, caused by changes in IOP, will result in changes in resonant frequency. When controlled in a small deflection regime,

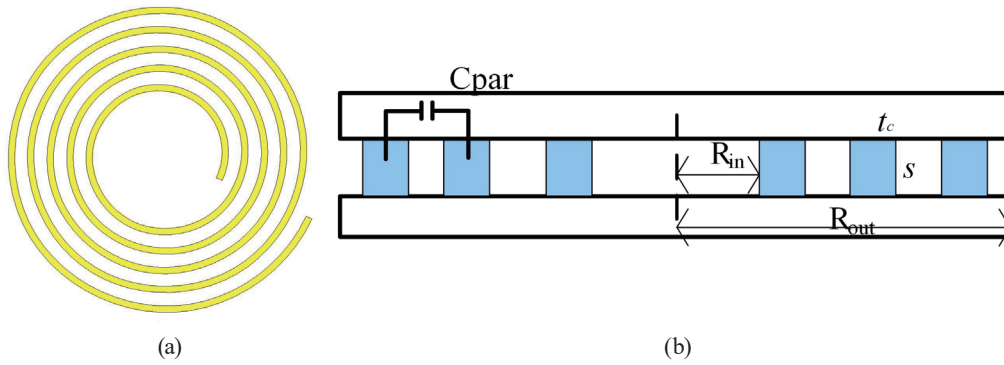


Fig. 2. (Color online) Schematic of sensor and parasitic capacitance. (a) Sensor schematic. (b) Diagram of sensor's parasitic capacitance.

depending on design parameters, the diaphragm deformation profile under a pressure load can be described as

$$\omega(r) = \frac{\Delta P a^4}{64D} \left[1 - \left(\frac{r}{a} \right)^2 \right]^2, \quad (11)$$

where ΔP is the pressure difference across the diaphragm, a is the diaphragm radius, and r is the radial coordinate from the center of the circular diaphragm. D is the flexural rigidity of the diaphragm, which is given by

$$D = Et^2 / [12(1-\nu^2)], \quad (12)$$

where E is Young's modulus of the diaphragm, ν is Poisson's ratio of the material, and t is the diaphragm thickness.

By combining Eqs. (1), (5), and (13), the relationship between the IOP and the frequency change of this designed IOP sensor is

$$\Delta P = - \frac{Et}{\pi^2 m a d_{avg} f_0^2 C_s R_0 (1-\nu)} \cdot \frac{\Delta f_0}{f_0}. \quad (13)$$

According to the above analysis, coil bending caused by changes in IOP will result in changes in resonant frequency. Figure 3 shows a schematic diagram of the cornea and the bending deformation of the sensor caused by a change in IOP.⁽¹⁹⁾

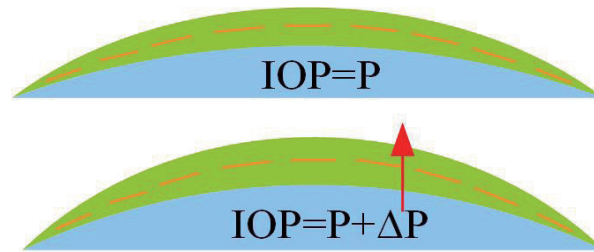


Fig. 3. (Color online) Diagram of the conceptual deformation of the proposed IOP sensor, when the pressure increases from P to $P + \Delta P$.

2.2 Design of the IOP sensor

The radius of curvature of a human cornea is 7.80 mm.⁽²⁰⁾ The image of light entering into the eye is determined by the size of the center of the iris. The diameter of a typical human pupil is about 2.5–4 mm. We designed an IOP sensor with a coil diameter of 7.5 mm and the diameter of the center transparent area of 5 mm, making it suitable for human eyes. The coil width of the inductor is 0.5 mm, and the space between adjacent coil leads is 0.5 mm.

The RF simulation software Agilent ADS is utilized to model the coupled resonant frequency in different situations. The number of turns in the sensor and antenna, and the response when the sensor is not deformed are considered. A three-dimensional model of the sensor and antenna is shown in Fig. 4. The IOP sensor has five turns and the antenna has two turns. The centers of the sensor and antenna are coincident and are placed parallel to each other, with a coupled distance of 10 mm. The sweep range of the antenna is set to 400–1000 MHz.

Figure 5 illustrates the results of simulations considering three, four, and five turns in the sensor. From Fig. 5, it can be seen that the resonant frequency decreases in response to an increase in the number of turns of the coil. Moreover, the pulse width with a mutation of the curve becomes smaller, and the peak of the curve becomes sharper. Although the lower resonant frequency and sharper peak can be detected more easily by the network analyzer, the typical size of human eyes and the production resolution limit the possibility of fabricating a sensor with more turns. Consequently, a coil with five turns was fabricated and tested in this study. The resonant frequency decreased from 885 to 532 MHz.

2.3 Fabrication of the IOP sensor

As shown in Fig. 6, the fabrication steps for the proposed IOP sensor are as follows. Figure 6(a) depicts the cleaning of the silicon used as a substrate for the PDMS sensor. As seen in Fig. 6(b), the silicon substrate was silylated in a 1% solution of 1H,1H,2H,2H-perfluorooctyl-trichlorosilane in toluene. Next, the silicon substrate was spin-coated with a 20- μm -thick layer of PDMS (Dow Corning SYLGARD184), as depicted in Fig. 6(c). Then, the PDMS substrate was spin-coated with a 10- μm -thick layer of photoresist (AZ 4620), as seen in

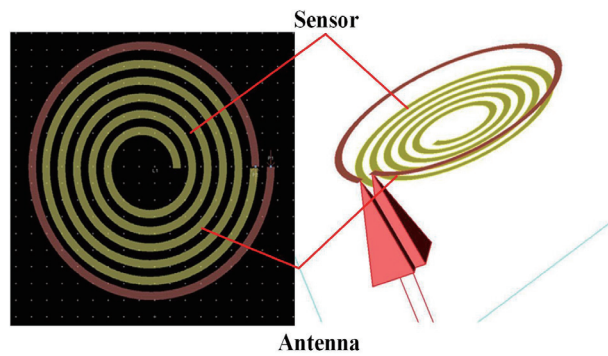


Fig. 4. (Color online) Three-dimensional model of the sensor and antenna.

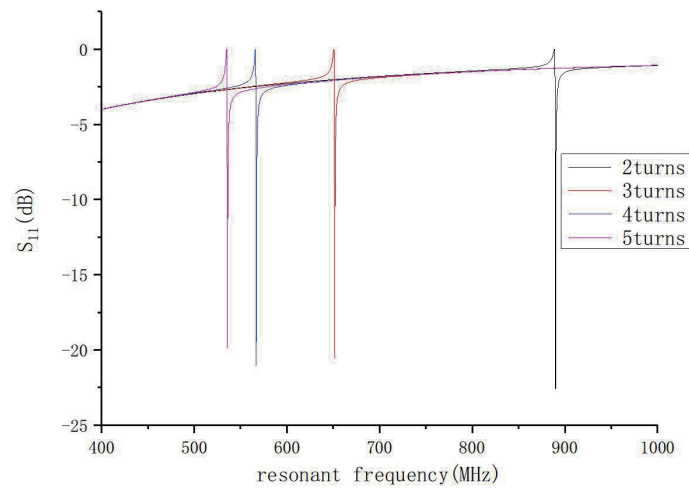


Fig. 5. (Color online) Results of simulations considering the number of turns in the sensor.

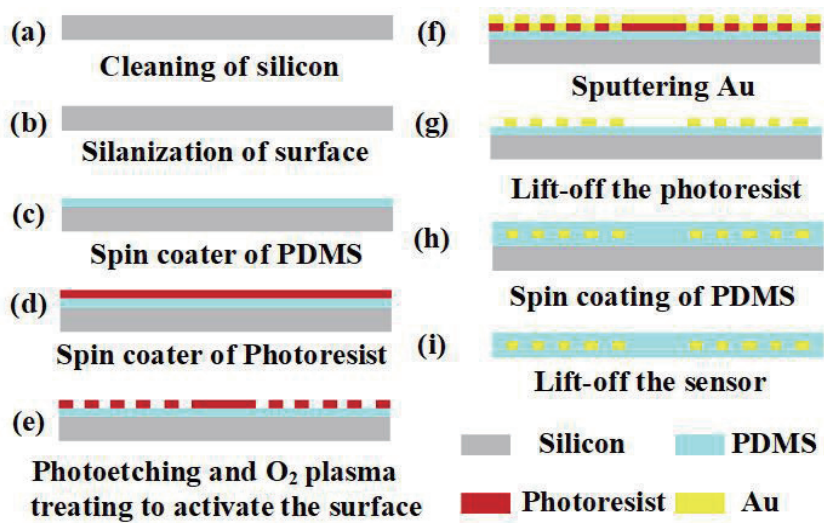


Fig. 6. (Color online) Fabrication process of the IOP sensor.

Fig. 6(d). Following photolithography processes, including exposure and development, the PDMS substrate was treated using O_2 plasma, as in Fig. 6(e). A 1- μm -thick gold layer was then evaporated on the PDMS substrate, as shown in Fig. 6(f). The photoresist was removed through lift-off, as shown in Fig. 6(g). Following this, the sensor was again spin-coated with PDMS to create a protective layer, as in Fig. 6(h). Finally, the supporting silicon substrate was removed, and the IOP sensor was fabricated, as depicted in Fig. 6(i). We need only a single lithography and sputtering process, effectively improving the probability of success of the experiment.

3. Test and Analysis

A schematic diagram of the experimental test platform is shown in Fig. 7(a). The fabricated test platform is shown in Fig. 7(b). The soft inductor–capacitor (LC) IOP sensor is placed on an artificial eye model. A burette is connected to a polytetrafluoroethylene (PTFE) capillary tube to control the flow of water to the artificial eye. The model bionic eye is fabricated by bonding a PDMS membrane to the PDMS base with a cavity. Although the artificial eye is similar to a human eye in shape, size, and corneal variation, it differs in flexibility and texture. The diameter of the artificial eye is 14 mm. The artificial eye model and attached sensor are placed in the test system. An antenna is fixed above the sensor at a distance of 10 mm, two ports of which are connected to a network analyzer (Agilent E5061B, Agilent Technologies, Santa Clara, CA, USA). During testing, we detect the water pressure inside the model eye using the communicating vessels principle and equate this to the height of the water column. We control the pressure of the model eye by changing the height of the water column, which is initially 10 cm. We increase the height of the water column in 5 cm increments, changing the pressure inside the eye, until it is balanced with the pressure of the burette. When the water column rises, the internal pressure of the artificial eye increases immediately, which results in the artificial eye deformation, and the radius of curvature of the artificial eye changes. The IOP sensor is attached tightly and the sensor is deformed. We measure the resonant frequency of the IOP sensor using a network analyzer and register the corresponding pressure of the eye model.

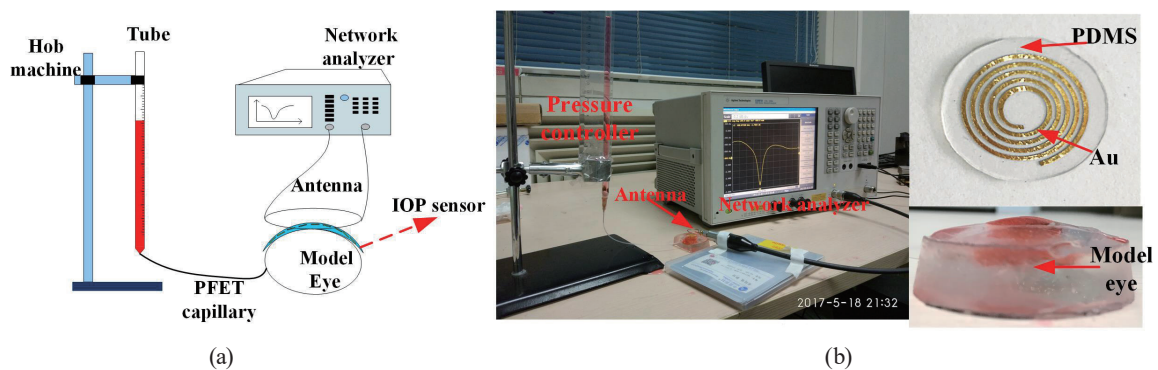


Fig. 7. (Color online) Test platform for the IOP sensor. (a) Schematic diagram of the test platform for the IOP sensor. (b) Fabricated test platform.

In order to verify the flexible performance of the sensor and ensure that the sensor has good signal in the intraocular pressure test, the sensor is tested for bending. We folded the sensor in half, as shown in Fig. 8(a). We then observed that the circuit, which was embedded in the PDMS, was intact, as shown in Fig. 8(b). This is because, when gold is sputtered on the surface of the PDMS, there is a large difference between the thermal expansion coefficients of the two materials. As a result, the coil is wrinkled, but the gold has excellent ductility compared with other metals, such as copper and silver. In addition, we utilized O₂ plasma treatment on the surface of the PDMS, which enhanced the adhesion of the gold film.

In the IOP test, we set the frequency sweep range from 550 to 650 MHz and the fundamental resonant frequency to 605 MHz. To measure the resonant frequency of the sensor with different pressures applied, we identified each pressure, as shown in Fig. 9(a). We registered thirteen data sets for each measurement and used Origin software to obtain the relationship between pressure and resonant frequency. The variation in resonant frequency, measured with the network analyzer and model eye pressure, is shown in Fig. 9(b). The sensor was tested under

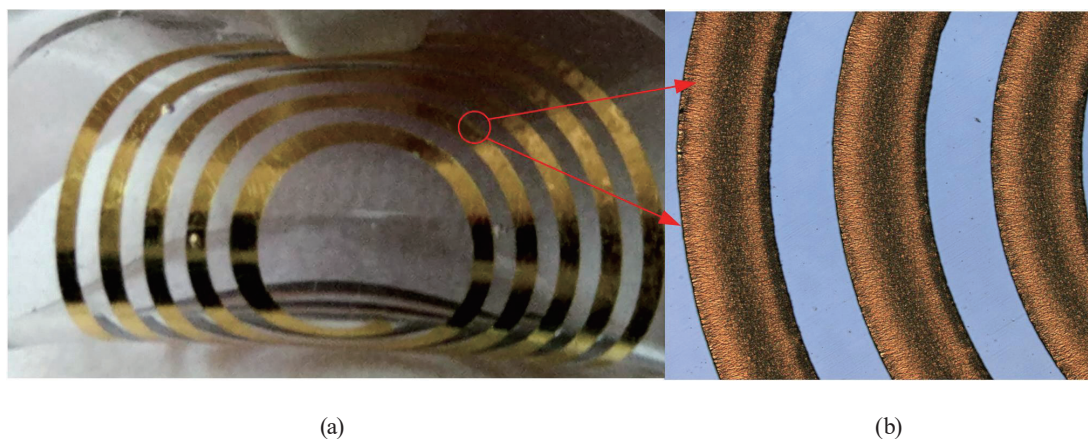


Fig. 8. (Color online) Illustration of IOP sensor bending test. (a) Bending test and (b) microgram of sensor.

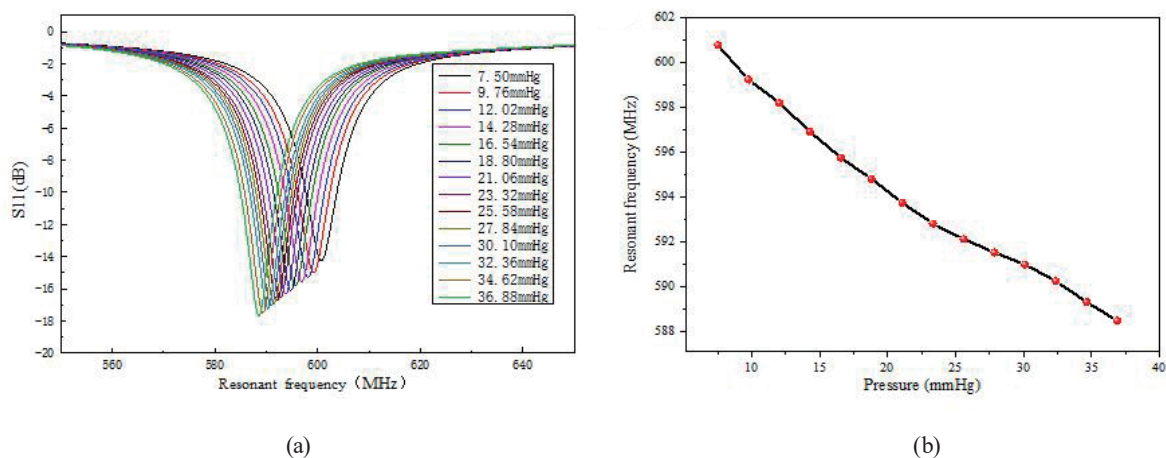


Fig. 9. (Color online) (a) Data recorded by the network analyzer. (b) Relationship between pressure and resonant frequency.

different pressures and the error bar is fitted in Fig. 9(b). From these results, we concluded that the resonant frequency decreases with increasing pressure. Compared with the simulated results, the experimentally recorded resonant frequencies and the corresponding amplitudes of the S_{11} parameters are much smaller. This reduction is a result of a number of factors related to the referenced parameters used in the simulation, such as the characteristic impedance of the sensor and network analyzer, and the dielectric constant of the substrate of the sensor, and the implicit assumption that these parameters are ideal. In contrast, the parameters of the fabricated sensor may have deviated from the referenced values. The pressure of the artificial eye module ranged from 7.50 to 36.88 mmHg.

From the above results, we can conclude that, in the pressure range used, there is an approximate linear relationship between the pressure and the resonant frequency. Input pressures between 7.50 and 36.88 mmHg result in resonant frequencies between 600.76 and 588.50 MHz, which yield a sensitivity of 417.29 kHz/mmHg. Similar resonant frequencies were observed after repeating the experiments using the same input pressures, showing that the response of the sensor is reproducible and stable after different cycles of increasing and decreasing pressure.

From the above analysis, it can be seen that a simplified IOP sensor structure, designed with only one inductor coil, is feasible for monitoring the IOP, as the parasitic capacitance between the coil leads is sufficient for creating an LC resonant circuit. The geometry of the IOP sensor simplifies the fabrication process and sensor structure. Consequently, the sensor proposed in this paper is promising for use in IOP detection in the future.

4. Conclusions

Increases and fluctuations in pathological IOP are the primary causes of glaucoma. Thus, the accurate real-time monitoring of IOP plays an important role in diagnosing eye diseases. We proposed an IOP sensor based on the LC resonant coupling principle, composed solely of a single spiral inductor, which can monitor the IOP in real time. The sensing elements were fully embedded into PDMS via MEMS technology. The experimental results showed that the measured resonant frequency has a negative linear correlation with the IOP. The sensitivity of the device was about 636.1 kHz/mmHg. Thus, the sensor can accurately track fluctuations of intraocular pressure using the calibrated relationship between the frequency response and the IOP for a short term. Moreover, the changes in resonant frequency can be transferred to medical terminals via a wireless coupling device. This soft contact lens device allows for simplified sensor configuration and manufacturing process. The IOP sensor has great potential for wireless 24 h IOP monitoring and contributes to the early detection of glaucoma and a timely remedy for patients. The device also has potential applications in blood pressure and cardiovascular pressure measurements. In the future, we will utilize the near-field communication (NFC) function of the smartphone to detect the IOP, and we must write a dedicated program to show changes in IOP. It will be portable for glaucoma patients and more suitable for the 24 h continuous monitoring of the IOP. Moreover, there may be many challenges, such as how to transmit signals within the biological tissue, but we will continue to optimize the design of the sensor, which can be more suitable for monitoring the eye pressure continuously.

Acknowledgments

This work was supported by the Program for the Top Young Academic Leaders of Higher Learning Institutions of Shanxi Province, China, and the Outstanding Youth talents Program of Shanxi Province sponsored by the Fund for Shanxi '1331 Project' Key Subject Construction.

Conflicts of Interest

The authors declare no conflicts of interest.

References

- 1 G. Chitnis, T. Maleki, and B. Samuels: *IEEE Trans. Biomed. Eng.* **60** (2013) 250
- 2 P. J. Chen, D. C. Rodger, and R. Agrawal: *J. Micromech. Microeng.* **17** (2007) 1931.
- 3 Y. Lawrence, J. K. Brian, and M. Ellis: *Sensors* **14** (2014) 20620.
- 4 J. C. Chiou, Y. C. Huang, and G. T. Yeh *J. Micromech. Microeng.* **26** (2015) 015001.
- 5 E. Hughes and P. Spry: *Diamond J. Glaucoma* **12** (2003) 232.
- 6 G. D. Chitnis, T. Maleki, B. Samuels, L. B. Cantor, and B. Ziaie: *Proc. IEEE Int. Conf. Micro Electro Mechanical Systems (MEMS)* (2012) 922.
- 7 G. Z. Chen, I. S. Chan, and L. K. Leung: *Med. Eng. Phys.* **36** (2014) 1134.
- 8 M. H. Ghaed, G. Chen, and R. Haque: *IEEE Trans. Circuits Syst. I: Regular Papers* **60** (2013) 3152.
- 9 R. M. Haque: *An Implantable Microsystem for Autonomous Intraocular Pressure Monitoring*, University of Michigan (2011).
- 10 P. Zeng, Q. Cui, M. Wu, P. Y. Chen, and M. C. Cheng: *Sensors 2016 IEEE (IEEE, 2016)* 1–3.
- 11 L. Yu, B. J. Kim, and E. Meng: *Sensors* **14** (2014) 20620.
- 12 L. T. Ee, N. N. Wen, and Y. S. Ran: *Sensors* **7** (2007) 1747.
- 13 H. Kang, Q. L. Tan, and L. Qin: *Chin. J. Sens. Actuators* **26** (2013) 498.
- 14 T. Luo, M. L. Yang, and Q. L. Tan: *Chin. J. Sens. Actuators* **27** (2014) 327.
- 15 M. A. Fonseca: *Dissertations & Theses – Gradworks*, Georgia Institute of Technology, Atlanta, 2007.
- 16 C. P. Yue and S. S. Wong: *IEEE Trans. Electron Devices* **47** (2000) 560.
- 17 P. Berest: *Eur. J. Mech. A. Solids* **9** (1990) 84.
- 18 U. M. Jow and M. Ghovanloo: *IEEE Trans. Biomed. Circuits Syst.* **1** (2007) 193.
- 19 P. J. Chen, S. Saati, and R. Varma: *J. Microelectromech. Syst.* **19** (2010) 721.
- 20 V. Laukhin, I. Sánchez, and A. Moya: *Sens. Actuators, A* **170** (2010) 36.